

Spin Wave Theory of Double Exchange Ferromagnets

D. I. Golosov

NORDITA, Blegdamsvej 17, DK-2100 Copenhagen Ø, Denmark

We construct the spin-wave ($1/S$) expansion for double exchange ferromagnets at $T=0$. It is assumed that the value of Hund's rule coupling, J_H , is sufficiently large, resulting in a fully saturated, ferromagnetic half-metallic ground state. We evaluate corrections to the magnon dispersion law, and we also find that, in contrast to earlier statements in the literature, magnon-electron scattering does give rise to spin wave damping. We analyze the momentum dependence of these quantities and discuss the experimental implications for colossal magnetoresistance compounds.

PACS numbers: 75.30.Vn, 75.30.Ds, 75.10.Lp

The phenomenon of colossal magnetoresistance (CMR), with its potential technological applications, has motivated an extensive experimental and theoretical research effort directed at the understanding of properties of doped manganese oxides [1]. In particular, considerable attention has been paid to magnetic properties of these compounds. An ubiquitous feature shared by the numerous theoretical models of the CMR compounds is the presence of a strong ferromagnetic Hund's rule exchange coupling, J_H , between the spins of itinerant e_g electrons and the core spins of Mn ions. The kinetic energy of itinerant electrons is then minimized when the ionic spins are parallel to each other; this gives rise to the conduction-electron mediated *double exchange* ferromagnetism [2]. The physics of double exchange is thus completely different from that of both Heisenberg exchange and RKKY interaction (the latter corresponding to the case of small J_H).

Since the value of core spin is relatively large, $S = 3/2$, studying the effects of double exchange interaction in the large- S (spin-wave) limit should provide at least qualitative description of the low-temperature properties of the manganites. At the same time, quantum nature of the core spins does affect the behaviour of the system in a profound way, as indicated by the variational results [6]. At finite S , the continuum of Stoner-like single-particle excitations with finite energies is present even at $J_H \rightarrow \infty$; also, the spin wave spectrum obtained variationally shows a non-trivial dependence on S . It is therefore somewhat surprising that, apart from the leading-order calculations [3–5] (which do not account for any quantum-spin corrections), the spin wave theory of double exchange magnets remains undeveloped. The objective of the present paper is to partially fill this gap. We will show that the subleading terms in the $1/S$ expansion, which originate from magnon-electron scattering, provide corrections to the magnon dispersion law, and also give rise to magnon damping. We will also see how the momentum dependence of these quantities is affected by the Fermi surface geometry. The relevant experimental data

will be discussed briefly.

We start with the standard double exchange Hamiltonian,

$$\mathcal{H} = -t \sum_{\langle i,j \rangle, \alpha} c_{i\alpha}^\dagger c_{j\alpha} - \frac{J_H}{2S} \sum_{i,\alpha,\beta} \vec{S}_i \vec{\sigma}^{\alpha\beta} c_{i\alpha}^\dagger c_{i\beta}. \quad (1)$$

Here $c_{j\alpha}$ are the electron annihilation operators, \vec{S}_i are the operators of the core (localized) spins located at the sites of a square (or simple cubic) lattice, and the vector $\vec{\sigma}^{\alpha\beta}$ is composed of Pauli matrices. We assume, for simplicity, that only one conduction-electron orbital (with two possible values of spin projection, $\alpha = \uparrow, \downarrow$) is available per each site i . Throughout the paper we use units in which hopping t , \hbar , and the lattice spacing are all equal to unity, and we consider the $T = 0$ case.

There is presently no reason to doubt that for $S \geq 3/2$ the ground state of the Hamiltonian (1) is ferromagnetic, at least for an infinite system in two or three dimensions and with a finite number of electrons per site, $x < 1$ (this is corroborated by the variational calculations [6,7]; see also Ref. [8] for the 1D case, and Ref. [9] for finite-size systems). The electron spectrum in the ferromagnetic state is given by $\epsilon_{\vec{k}}^{\uparrow,\downarrow} = \epsilon_{\vec{k}} \mp J_H/2$, where for the tight-binding model of Eq. (1), $\epsilon_{\vec{k}} = -\sum_{a=1}^d \cos k_a$, and d is the dimensionality of the lattice. We will only consider the half-metallic case [10] when the chemical potential lies below the bottom of the upper band, $\epsilon_F < \frac{1}{2}J_H - d$, so that only spin-up electrons are present in the ground state.

The magnon operators a_i are introduced by means of the Holstein – Primakoff transformation, and the canonical transformation [5] $\mathcal{H} \rightarrow \mathcal{H}' = \exp(-U)\mathcal{H}\exp(U)$ with

$$\mathcal{U} = \frac{J_H}{\sqrt{2SN}} \sum_{\vec{k}, \vec{p}} \left(\frac{c_{\vec{k}\uparrow}^\dagger c_{\vec{k}+\vec{p}\downarrow} a_{\vec{p}}^\dagger}{\epsilon_{\vec{k}}^\uparrow - \epsilon_{\vec{k}+\vec{p}}^\downarrow} - \text{h.c.} \right) \quad (2)$$

(where N is the number of lattice sites and the summation is over the first Brillouin zone) is then applied to

the Hamiltonian, thereby accomplishing the transition to the “true magnons”. The resultant Hamiltonian can be written as an expansion in powers of $S^{-1/2}$:

$$\mathcal{H}' = \sum_{\vec{k}, \alpha} \epsilon_{\vec{k}}^{\alpha} c_{\vec{k}\alpha}^{\dagger} c_{\vec{k}\alpha} + \mathcal{H}'_2 + \mathcal{H}'_3 + \mathcal{H}'_4 + \dots . \quad (3)$$

Here, the term $\mathcal{H}'_1 \propto S^{-1/2}$ has been eliminated by the canonical transformation, and

$$\begin{aligned} \mathcal{H}'_2 = & -\frac{J_H^2}{2NS} \sum_{\vec{k}, \vec{q}} \frac{c_{\vec{k}\downarrow}^{\dagger} c_{\vec{k}\downarrow}}{\epsilon_{\vec{q}}^{\uparrow} - \epsilon_{\vec{k}}^{\downarrow}} + \frac{J_H}{4NS} \sum_{1,2,3,4} \left\{ \frac{c_{1\downarrow}^{\dagger} c_{2\uparrow}^{\dagger} c_{3\uparrow} c_{4\downarrow}}{\epsilon_2^{\uparrow} - \epsilon_4^{\downarrow}} + \right. \\ & \left. + \frac{\epsilon_1 - \epsilon_{1+3}}{\epsilon_1^{\uparrow} - \epsilon_{1+3}^{\downarrow}} c_{1\uparrow}^{\dagger} c_{2\uparrow} a_3^{\dagger} a_4 - \frac{\epsilon_{2-3} - \epsilon_2}{\epsilon_{2-3}^{\uparrow} - \epsilon_2^{\downarrow}} c_{1\downarrow}^{\dagger} c_{2\downarrow} a_3^{\dagger} a_4 + \text{h.c.} \right\}. \quad (4) \end{aligned}$$

Here, the subscripts 1, 2, ... stand for $\vec{p}_1, \vec{p}_2, \dots$, and \sum' means that the quasimomentum conservation law is enforced. The spin wave energy $\omega_{\vec{p}}$ is equal to the on-shell value of the real part of the magnon self energy (cf. Ref. [4]). The leading-order term in self energy, which originates from \mathcal{H}'_2 , is real and coincides with the earlier results [3–5], which in the $J_H \rightarrow \infty$ limit reduce to

$$\omega_{\vec{p}}^{(0)} = -\frac{1}{2S} \int n_{\vec{q}}(\epsilon_{\vec{q}} - \epsilon_{\vec{p}+\vec{q}}) \frac{d^d q}{(2\pi)^d}, \quad (5)$$

where $n_{\vec{q}}$ is the Fermi distribution function for the spin-up electrons. Using the explicit form for $\epsilon_{\vec{q}}$, one obtains a Heisenberg-like expression, $\omega_{\vec{p}}^{(0)} = |E|(d + \epsilon_{\vec{p}})/2dS$. Here, $E = \int \epsilon_{\vec{q}} n_{\vec{q}} d^d q / (2\pi)^d$ is the total energy of electrons calculated with respect to the center of the lower band.

Evaluation of the higher-order terms in Eq. (3) involves repeated commutations of the operator \mathcal{U} (see Eq. (2)) with the original Hamiltonian, Eq. (1). Among the numerous terms that are generated in this way, we need to select only those that have a non-vanishing average value in a one-magnon state [11]. Such terms do not occur in \mathcal{H}_3 , and we find

$$\begin{aligned} \mathcal{H}'_4^{\text{eff}} = & \frac{J_H^3}{32S^2N^2} \sum_{1 \div 6} \frac{c_{1\uparrow}^{\dagger} c_{2\uparrow}^{\dagger} c_{3\uparrow} c_{4\uparrow} a_5^{\dagger} a_6}{\epsilon_4^{\uparrow} - \epsilon_{4+6}^{\downarrow}} \left\{ \frac{1}{\epsilon_2^{\uparrow} - \epsilon_{4+6}^{\downarrow}} \left[4 + \right. \right. \\ & \left. \left. + \frac{2J_H}{\epsilon_1^{\uparrow} - \epsilon_{1+5}^{\downarrow}} + \frac{J_H}{\epsilon_3^{\uparrow} - \epsilon_{1+5}^{\downarrow}} \right] + \frac{J_H}{(\epsilon_1^{\uparrow} - \epsilon_{1+5}^{\downarrow})(\epsilon_3^{\uparrow} - \epsilon_{1+5}^{\downarrow})} \right\} - \\ & - \frac{J_H^3}{32S^2N^2} \sum_{1 \div 4} \frac{c_{1\uparrow}^{\dagger} c_{2\uparrow}^{\dagger} a_3^{\dagger} a_4}{\epsilon_2^{\uparrow} - \epsilon_{2+4}^{\downarrow}} \sum_{\vec{q}} \frac{1}{\epsilon_{\vec{q}}^{\uparrow} - \epsilon_{2+4}^{\downarrow}} \left[4 + \right. \\ & \left. \left. + \frac{3J_H}{\epsilon_1^{\uparrow} - \epsilon_{2+4}^{\downarrow}} + \frac{J_H}{\epsilon_{\vec{q}}^{\uparrow} - \epsilon_{2+4}^{\downarrow}} \right] + \text{h.c.} \right\}. \quad (6) \end{aligned}$$

Naturally, both \mathcal{H}'_2 and \mathcal{H}'_4 have well-defined $J_H \rightarrow \infty$ limits. In what follows we will for simplicity restrict ourselves to the case of infinite J_H ; straightforward generalization to the finite- J_H case can always be accomplished with the help of Eqs. (4) and (6).

The first quantum correction to the magnon self energy is proportional to S^{-2} and includes the first-order perturbative contribution from \mathcal{H}'_4 as well as second-order contribution $\Sigma_2(0, \vec{p})$ from \mathcal{H}'_2 (corresponding to the first diagram in Fig. 2 below):

$$\omega_{\vec{p}}^{(1)} = \frac{1}{16S^2} \int (3\epsilon_{\vec{q}} - 4\epsilon_{\vec{q}+\vec{p}}) n_{\vec{q}} \frac{d^d q}{(2\pi)^d} + \text{Re}\Sigma_2(0, \vec{p}), \quad (7)$$

$$\Sigma_2(\omega, \vec{p}) = \frac{1}{16S^2} \int \frac{(\epsilon_{\vec{q}} + \epsilon_{\vec{k}} - 2\epsilon_{\vec{p}+\vec{q}})^2 (1 - n_{\vec{k}}) n_{\vec{q}}}{\omega + \epsilon_{\vec{q}} - \epsilon_{\vec{k}} + i0} \frac{d^d q d^d k}{(2\pi)^{2d}}. \quad (8)$$

A result similar to Eq. (7) was published by Nagaev [12]. However, Eq. (7) contains additional terms which do affect the spectrum.

For a 2D system with band filling values $x = 0.3$ and $x = 0.4$, the quantity $\omega_{\vec{p}}^{(1)} S^2$ is plotted in Fig. 1 a (solid and dotted lines, respectively). The dashed lines represent the corresponding Heisenberg-like fits, $\tilde{\omega}_{\vec{p}}^{(1)} S^2 = 2D^{(1)}(2 + \epsilon_{\vec{p}})S^2$, where

$$D^{(1)} = \frac{1}{4S^2} \int \frac{(\partial \epsilon_{\vec{q}} / \partial q_x)^2}{\epsilon_{\vec{q}} - \epsilon_{\vec{k}}} (1 - n_{\vec{k}}) n_{\vec{q}} \frac{d^d q d^d k}{(2\pi)^{2d}} - \frac{x|E|}{8dS^2}$$

is the first quantum correction to spin stiffness. The deviation of $\omega_{\vec{p}}^{(1)}$ from $\tilde{\omega}_{\vec{p}}^{(1)}$ is not large, but it increases dramatically for smaller x , in agreement with the earlier numerical results [13].

The doping dependence of the spin stiffness, $D = D^{(0)} + D^{(1)}$, for $S = 3/2$ is shown in Fig. 1 b (solid line). The dashed line represents the leading-order term, $D^{(0)} = |E|/8S$. We see that for $S = 3/2$ the value of $D^{(1)}$ is not small numerically, implying that quantum corrections to the spin wave spectrum cannot be omitted in any quantitative treatment. Note that $D(x)$ is not symmetric with respect to quarter filling, $x = 0.5$, reflecting the loss of particle-hole symmetry at finite S .

Spin wave damping is given by the on-shell value of the imaginary part of magnon self energy, and the first-order perturbation theory terms obviously do not contribute to it. It is also easy to see that to second order in $1/S$, $\text{Im}\Sigma_2(\omega_{\vec{p}}, \vec{p}) = \text{Im}\Sigma_2(0, \vec{p}) = 0$. This is because the energies of all the intermediate states occurring in the second-order perturbation theory terms are higher than that of a single-magnon state (which to leading order equals the ground state energy). Therefore, the integration contour in the energy space terminates at the pole (cf. Eq. (8) with $\omega = 0$), so that the latter does not give rise to any imaginary contribution. In the third order in $1/S$, a multitude of new diagrams appear, combining all possible vertices from \mathcal{H}'_2 , \mathcal{H}'_3 , and \mathcal{H}'_4 . By the above reasoning, their leading-order imaginary parts vanish on shell [14], with one exception. This exception is the second diagram in Fig. 2, which corresponds to the term with the *second*-order pole in the standard third-order

perturbation theory formula [17]. This is nothing but a self energy correction to $\Sigma_2(\omega_{\vec{p}}, \vec{p})$ (Eq. (8)), and the net third-order contribution to the magnon relaxation rate is thus found from the diagram on the r. h. s. in Fig. 2:

$$\Gamma(\vec{p}) = \frac{\pi}{4S^2} \int J(\vec{p}, \vec{r}) \frac{d^d r}{(2\pi)^d}, \quad (9)$$

$$J(\vec{p}, \vec{r}) = \int (\epsilon_{\vec{q}} - \epsilon_{\vec{p}+\vec{q}})^2 (1 - n_{\vec{q}+\vec{r}}) n_{\vec{q}} \times \times \delta(\omega_{\vec{p}}^{(0)} - \omega_{\vec{p}-\vec{r}}^{(0)} + \epsilon_{\vec{q}} - \epsilon_{\vec{q}+\vec{r}}) \frac{d^d q}{(2\pi)^d}. \quad (10)$$

Note that $J(\vec{p}, \vec{r})$ is of the order of $1/S$.

The value $\Gamma(\vec{p})$ for different values of bandfilling x in the 2D case is plotted in Fig. 3. It shows strong momentum dependence, reaching (for $S = 3/2$) up to 10 % of the corresponding magnon energy. The fact that this quantity differs from zero in a $J_H \rightarrow \infty$, $T = 0$ pure double-exchange system is at variance with the prevalent view (see, *e. g.*, Refs. [15,16]). On the other hand, as one can readily see from Fig. 2, it is a direct consequence of magnon-electron scattering.

We note that Eqs. (9–10) (as well as Eqs. (2–8)) remain unchanged if the first term in the Hamiltonian (1) is written as $\sum_{\vec{k}, \alpha} \epsilon_{\vec{k}} c_{\vec{k}\alpha}^\dagger c_{\vec{k}\alpha}$ with an arbitrary $\epsilon_{\vec{k}}$. It is thus possible to use Eqs. (9–10) to evaluate $\Gamma(\vec{p})$ for an arbitrary single-band electron dispersion. The overall profile of $\Gamma(\vec{p})$ (as well as that of $\omega_{\vec{p}}$) is sensitive to both the carrier concentration value x and the details of electron bandstructure throughout the Brillouin zone. There are, however, certain generic features in the behaviour of $\Gamma(\vec{p})$:

1. Long-wavelength limit. When p is small in comparison to the Fermi momentum k_F , $\Gamma(\vec{p})$ is proportional to p^5 in the 2D case and to p^6 in three dimensions. Here, the factor p^2 originates from the matrix element $(\epsilon_{\vec{q}} - \epsilon_{\vec{p}+\vec{q}})^2$ in Eq. (10), and is multiplied by a p^d corresponding to the space volume available to the virtual magnon with momentum $\vec{p} - \vec{r}$ and energy $\omega_{\vec{p}-\vec{r}} < \omega_{\vec{p}} \approx D^{(0)} p^2$ (see Fig. 2). The remaining factor of p^1 comes from electron kinematics. In the one dimensional case, $\Gamma(p) \equiv 0$ everywhere at $p < k_F$.

2. The anomaly at $p = k_F$. The Fermi surface geometry manifests itself through a weak singularity of $\Gamma(\vec{p})$ at $p = k_F$ [18]. Indeed, the quantity $J(\vec{p}, \vec{r})$ (see eq. (10)) has a singularity at $r = 2k_F$, and vanishes at $\omega_{\vec{p}-\vec{r}}^{(0)} = \omega_{\vec{p}}^{(0)}$. The anomaly in $\Gamma(\vec{p})$ is due to the tangency between these two surfaces (in \vec{r} -space), which occurs at $p = k_F$. At this point, the second (in 2D) or third (in 3D) derivative of $\Gamma(p)$ suffers either a jump or a logarithmic divergence, depending on the local geometry of these two tangent surfaces. These singularities are too weak to be visible in Fig. 3, except for $x = .49$, when owing to the flatness of the Fermi surface the singularity acquires a nearly-1D (jump in the *first* derivative) character [19].

The anomaly in $\Gamma(\vec{p})$ is of course accompanied by a singularity in the third-order (in $1/S$) term in $\omega_{\vec{p}}$. It is contained in the real part of the same diagram, and for an isotropic dispersion law amounts to a jump in the second derivative (2D) or to a logarithmic divergence in either the first (1D) or third (3D) derivative of $\omega_{\vec{p}}$.

Taking into account the anticipated Fermi surface geometry of the CMR compounds [20], it is worthwhile to mention the case when the Fermi surface is nearly-cubic (nearly square). As the magnon isoenergetic surfaces are unlikely to have the same shape [21], this situation is not reducible to the 1D case. In fact, when the vector \vec{p} is perpendicular to a flat part of the Fermi surface, the singular term in $\Gamma(\vec{p})$ is proportional to $(p - k_F)^{3/2} \theta(p - k_F)$ in 2D and to $(p - k_F)^2 \theta(p - k_F)$ in 3D. The corresponding singularity in $\omega_{\vec{p}}$ is given by $-(p - k_F)^{3/2} \theta(p - k_F)$ in 2D and by $(p - k_F)^2 \ln|p - k_F|$ in 3D.

Some comments are in order concerning the experimental situation. Low temperature spin dynamics, including spin wave damping and the deviation of magnon spectrum from the Heisenberg-like form, is studied intensively in both 3D perovskite [16,22,23] and quasi-2D layered [24] CMR manganites. In both cases, unexpectedly large low- T values of $\Gamma(p)$ at large p were found, which is consistent with our results (in some compounds [23], $\Gamma(p)$ may be due in part to electron-phonon coupling). However, the lack of detailed knowledge of electron bandstructure restricts one's options in comparing theoretical and experimental results quantitatively.

The low-momentum measurements of $\Gamma(\vec{p})$ in the perovskite manganites [16] yield the $p^4 [T \ln(T/\omega_p)]^2$ dependence, attributable to the magnon-magnon scattering. We suggest that these measurements, both in 2D and 3D compounds, should be performed at lower temperatures in order to reveal the p^5 or p^6 contribution of magnon-electron scattering (which is likely to have a numerically small prefactor [25]). Once more data about the Fermi surface become available, one should also try to identify the $p = k_F$ anomalies in Γ and ω (the irregularity seen in the data of Ref. [16] at $p \sim \pi/2$ may be a possible candidate).

We also suggest that a systematic study of doping dependence of spin stiffness should be performed, in particular, in the layered compounds. We note that our results for $D(x)$ in Fig. 1 *b* may be not inconsistent with the measured doping dependence of the Curie temperature [26] (with $T_C(x)$ passing through a maximum at $x \approx .37$), but a direct comparison with the experimental data for D would be highly desirable.

In conclusion, we have calculated the spin wave linewidth and correction to the spin wave energy for a double exchange half-metallic ferromagnet. The proposed new measurements would verify to what extent the double exchange model accounts for the low-temperature spin dynamics of the CMR compounds.

It is a pleasure to thank A. Luther for the many en-

lightening discussions and steady encouragement. Earlier discussions with K. Levin, M. R. Norman, and R. Osborn are also gratefully acknowledged.

[1] Physics of manganites, T.A. Kaplan and S. D. Mahanti, eds., (New York, Kluwer Academic/Plenum, 1999).

[2] P.-G. De Gennes, Phys. Rev. **118**, 141 (1960).

[3] E. L. Nagaev, Sov. Phys. Solid State **11**, 2251 (1970).

[4] N. Furukawa, J. Phys. Soc. Jpn. **65**, 1174 (1996).

[5] E. L. Nagaev, Phys. Rev. **B58**, 827 (1998).

[6] T. Okabe, Progr. Theor. Phys. **97**, 21 (1997).

[7] R. E. Brunton and D. M. Edwards, J. Phys.: Condens. Matter, **10**, 5421 (1998).

[8] K. Kubo, J. Phys. Soc. Jpn. **51**, 782 (1982).

[9] J. Zang *et al*, J. Phys.: Condens. Matter **9**, L157 (1997).

[10] This is appropriate for the CMR compounds (see, *e. g.*, J.-H. Park *et al*, Nature, **392**, 794 (1998)).

[11] This selection process is greatly simplified by the fact that there are no spin-down electrons in the ground state.

[12] E. L. Nagaev, Sov. Phys. JETP, **29**, 545 (1969).

[13] T. A. Kaplan and S. D. Mahanti, J. Phys.: Condens. Matter, **9**, L291 (1997).

[14] We note that the imaginary parts of the third-order (in \mathcal{H}'_2) ladder diagrams for the self energy behave as $S^{-3}\omega\ln\omega$, with the overall sign depending on momentum as well as on the details of the bandstructure. As for $\text{Im}\Sigma_2(\omega, \vec{p})$, it is proportional to $S^{-2}\omega\theta(\omega)$, and thus has to be included in the third-order (in $1/S$) on-shell calculation (see Fig. 2).

[15] N. Furukawa and K. Hirota, Physica **B241**, 780 (1997).

[16] L. Vasiliu-Doloc *et al*, Phys. Rev. **B58**, 14913 (1998).

[17] L. D. Landau and E. M. Lifshits, Quantum Mechanics (Course of Theoretical Physics Vol.3), Pergamon, Oxford, 1977, Sect. 38, Problem 2.

[18] Strictly speaking, the anomaly is located at a given point \vec{p} of the Fermi surface only when the electron velocity at this point is parallel to the magnon one, $\partial\epsilon_{\vec{q}}/\partial\vec{q} \parallel \partial\omega_{\vec{q}}^{(0)}/\partial\vec{q}$ at $\vec{q} = \vec{p}$. This holds, in particular, along any symmetry direction, or for the tight-binding model of Eq. (1).

[19] We also note that in 1D and in the absence of *Umklapp* processes, $\Gamma(2k_F) = 0$. Thus for $x = 0.49$, the value of $\Gamma(\pi, \pi)$ is small (see Fig. 3).

[20] D. S. Dessau *et al*, Phys. Rev. Lett. **81**, 192 (1998), and references therein; W. E. Pickett and D. J. Singh, J. Magn. Magnetic Mat., **172**, 237 (1997).

[21] The Fermi surfaces proposed for the CMR compounds [20] are parallel to the Brillouin zone boundary, thus they are not described by the tight-binding model of Eq. (1). The shapes of isoenergetic surfaces for electrons and magnons may then differ already in the leading order in $1/S$.

[22] J. A. Fernandez-Baca *et al*, Phys. Rev. Lett. **80**, 4012 (1998).

[23] P. Dai *et al*, preprint cond-mat/9904372 (1999).

[24] H. Fujioka *et al*, preprint cond-mat/9902253 (1999).

[25] For $\epsilon_{\vec{k}} \propto k^2$ and $p \ll k_F$, we find $\Gamma = Dk_F p^5/(90\pi^3 S^2)$ in 2D and $\Gamma = Dk_F^2 p^6/(1680\pi^3 S^2)$ in 3D.

[26] M. Kubota *et al*, preprint cond-mat/9901211 (1999).

FIG. 1. (a) The leading $1/S$ -corrections to the spin wave energy in a 2D system with carrier concentration $x = 0.3$ (solid line) and $x = 0.4$ (dotted line) as functions of momentum. The dashed lines represent respective Heisenberg-like fits, $\tilde{\omega}^{(1)} S^2$. (b) Doping dependence of spin stiffness D in a 2D system with $S = 3/2$. The dashed line corresponds to the classical value, $D^{(0)}$.

FIG. 2. Magnon self energy diagrams. Dashed and solid lines are the unperturbed Green's functions of magnons, $(\omega + i0)^{-1}$, and of the spin-up electrons, respectively. The bold dashed line is the exact magnon Green's function, which to required accuracy is given by $(\omega - \omega_{\vec{p}}^{(0)} + i0)^{-1}$. The boxes represent the interaction, *i.e.* the $c_{\uparrow}^{\dagger}c_{\uparrow}a^{\dagger}a$ -terms in Eq. (4).

FIG. 3. Momentum dependence of spin wave damping, $\Gamma(\vec{p})$, for a 2D system with $x = 0.3$, $x = 0.4$, and $x = 0.49$ (solid, dotted and dashed lines, respectively). The Fermi surface corresponds to $\vec{p} = (0.66\pi, 0)$ and $(0.42\pi, 0.42\pi)$ at $x = 0.3$, $(0.79\pi, 0)$ and $(0.47\pi, 0.47\pi)$ at $x = 0.4$, and $(0.95\pi, 0)$ and $(0.498\pi, 0.498\pi)$ at $x = 0.49$.

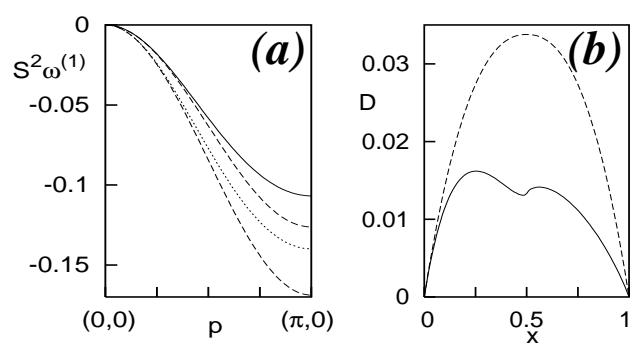


Fig. 1

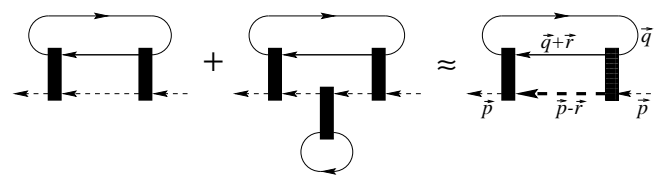


Fig. 2

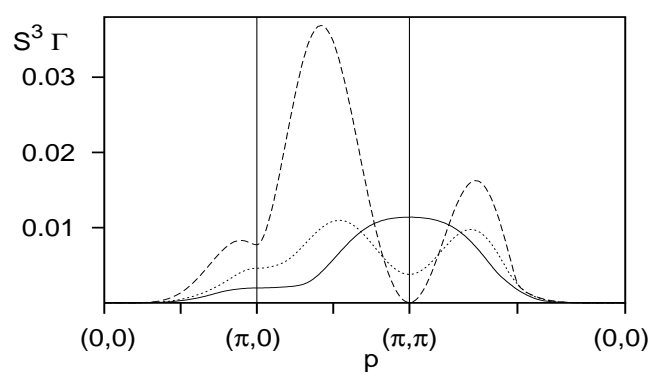


Fig. 3